

Microstructure and Mechanical Properties of Aluminum-Alumina Bulk Nanocomposite Produced by a Novel Two-Step Ultrasonic Casting Technique



H.M. VISHWANATHA, JAYAKUMAR ERAVELLY, CHERUVU SIVA KUMAR,
and SUDIPTO GHOSH

An unprecedented uniform distribution of nano-dispersoids in aluminum-alumina bulk nanocomposite and enhancement in mechanical properties were achieved through a novel ultrasonic casting technique involving two-step ultrasonication. Ultrasonic casting can be classified into two types: (a) contact type, in which the sonicating probe is in direct contact with the liquid melt during ultrasonication and (b) non-contact type, in which the ultrasonic waves reach the liquid melt through the mold wall. Each of the processes has certain disadvantages, and the present study aims at eliminating the primary disadvantages of both the processes, through a novel two-step ultrasonic casting technique. The significant improvement in distribution was possibly due to the cavitation in the mold, leading to the elimination of non-uniformity in the cooling rate at the mesoscopic scale. The improvement in mechanical properties is explained through microstructure analysis in correlation with EBSD analysis, TEM analysis, hardness test, and tensile test. The yield strength of the nanocomposite produced by the two-step process was ~38 pct higher than that produced by non-contact and contact methods.

DOI: 10.1007/s11661-016-3740-z

© The Minerals, Metals & Materials Society and ASM International 2016

I. INTRODUCTION

THE unabated thirst for fuel saving and cost-efficient materials in automotive, defence, and aerospace industries has made the researchers to focus on metal matrix composites (MMCs). Over the last few decades, MMCs reinforced with nano-dispersoids are gaining particular attention.^[1–3] Such metal matrix nanocomposites (MMNCs) are isotropic in nature and possess enhanced mechanical, thermal, and structural properties. MMNCs are produced *via* several routes.^[4–9] Casting and solidification processing method is found to be not only an economical way but also an efficient way for the production of bulk composites. However, achieving uniform distribution of the nano-dispersoids in the metal matrix through the solidification processing method remains a major challenge due to the density difference between the liquid metal and the solid ceramic particles.

The characteristic nature of the high surface-to-volume ratio and strong Van der Waals forces between the nano-dispersoids keep it in agglomerated state. Thus,

very high forces are required to break the bonds and thereby deagglomerate the clusters.^[10,11] Neither mechanical stirring nor such other type process can result in complete deagglomeration and uniform distribution of nano-dispersoids in the matrix. However, it is found that ultrasonic waves transmitted into the liquid melt (containing agglomerates of nano-dispersoids) can break the strong bonds and deagglomerate clusters of nano-dispersoids.^[12] When the solidification follows the dispersion, the process can be referred to as ultrasonic casting.

Ultrasonic casting can be of two types: contact type^[13–18] and non-contact type.^[1–3] In the case of contact type ultrasonic casting, the ultrasonic probe is in direct contact with the liquid melt present inside the furnace. The advantage of this method is that the ultrasonication (the process of melt treatment using high-energy ultrasonic waves) can be carried out for a longer duration of time. On the other hand, the contamination of the liquid melt as a result of direct contact between the probe tip and the liquid melt is a severe problem.

An alternative method was proposed to resolve the problem of contamination, called as non-contact type ultrasonic casting^[1] to produce bulk MMNCs. In this type of ultrasonic casting, the probe is not in direct contact with the liquid melt, but the acoustic energy to the liquid melt is transmitted through the mold wall. The drawback of this method is that there is a lack of sufficient time for complete deagglomeration. On the other hand, recently, a mathematical model was proposed regarding the breaking of agglomerates during non-contact ultrasonic casting.^[3]

H.M. VISHWANATHA, Doctoral Student, JAYAKUMAR ERAVELLY, MS Research Scholar, and SUDIPTO GHOSH, Professor, are with the Department of Metallurgical and Materials Engineering, Indian Institute of Technology-Kharagpur, Kharagpur, 721302, India. Contact e-mail: sudipto@metal.iitkgp.ernet.in CHERUVU SIVA KUMAR, Professor, is with the Department of Mechanical Engineering, Indian Institute of Technology-Kharagpur, Kharagpur, WB, 721302, India.

Manuscript submitted March 3, 2016.

Article published online September 6, 2016

In the present work, in addition to the above-mentioned two types of ultrasonic casting, *viz.* contact and non-contact types, a newer method involving two ultrasonication steps have been explored, with the aim of achieving maximum deagglomeration and uniform distribution of nano-dispersoids in the bulk MMNCs.

II. EXPERIMENTAL PROCEDURE

Pure aluminum of commercial grade (composition given in Table I) and alumina nano-dispersoids (Sigma-Aldrich, ~13 nm average size) were used for producing Al-1 wt pct Al₂O₃ bulk nanocomposites. Ingots were ultrasonically cast in three different ways: (a) two-step contact–non-contact ultrasonic casting, (b) contact type ultrasonic casting, and (c) non-contact type ultrasonic casting.

The two-step contact–non-contact ultrasonic casting of Al–Al₂O₃ MMNCs involves two ultrasonication steps. It was carried out in a specially designed casting setup as shown in Figure 1.

Initially, a graphite crucible was filled with alternate layers of calculated amount of Al₂O₃ nano-dispersoids and aluminum pieces, stacked upon one another as shown in Figure 1. Later on, the charged crucible was placed inside the melting chamber. The temperature of the furnace was gradually raised to 1023 K (750 °C). Preheating of the nanopowder would enhance the wettability of the nano-dispersoids with liquid melt.^[4,19,20] Thus, in the present work, the particles got heated up along with alumina pieces which possibly increased the wettability of alumina particles with the liquid melt. Also, in case of the feeding technique used in the present work, there is no escape of nanoparticles due to fumes as in the case of top feeding. Once the melting was completed, the top oxide slag layer was removed, and the ultrasonic probe (SONOPROS PR1000MP, 20 kHz, 1000 W) was gradually dipped into the liquid melt. When the tip of the probe comes in contact with the liquid melt, the ultrasonication was activated. Simultaneously, an electrical stirrer was also dipped into the liquid melt. The ultrasonication and stirring of the liquid melt were carried out for about 20 minutes and finally the liquid mixture was bottom poured through the tapping hole present at the bottom of the crucible. The liquid mixture was made to flow through the coiled tubular runner maintained at 1023 K (750 °C) and eventually drained into the stainless steel mold (thickness of 24 gauge) placed in an ultrasonic chamber (Bandelin RK100H, 35 kHz). The ultrasonic chamber was activated before the pouring was initiated. Thus, well before the start of the solidification, the ultrasonic waves were transmitted into the liquid melt inside the mold, and were continued till the end of the

solidification. The two-step contact–non-contact ultrasonic casting will be referred to as two-step process hereafter.

MMNCs were cast by the contact type ultrasonic casting. In this process, only the liquid melt containing nano-dispersoids was subjected to ultrasonication (top half of Figure 1) and no ultrasonication was provided once the liquid melt was poured into the mold. The contact type ultrasonic casting technique adopted in the current work is slightly different than that adopted by other research groups.^[13–18] MMNCs were also cast by non-contact type ultrasonic casting. In this process, once the contents in the mold were melted, the melt was subjected to stirring. No ultrasonication was provided during stirring. The stir mixed liquid melt was subjected to ultrasonication, only after it has been poured into the mold placed inside the ultrasonic chamber (bottom half of Figure 1). The details of the non-contact process adopted in the present study are different than that adopted by other research groups.^[1–3]

The cast ingots were sectioned into different zones as shown in Figure 2. The samples were ground

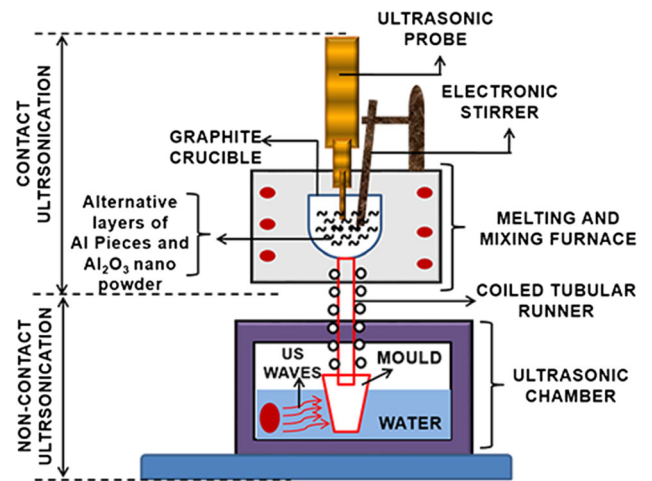


Fig. 1—Schematic representation of two-step contact–non-contact ultrasonic casting system.

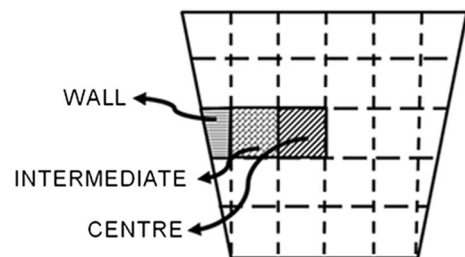


Fig. 2—Schematic showing the different zones of the sectioned cast ingot.

Table I. Composition of Commercial Pure Aluminum

Material	Al (Pct)	Si (Pct)	Mg (Pct)	Cr (Pct)
Commercial Pure Al	balance	0.26	0.43	0.96

successively on 180, 220, 400, 600, 800, and 1200 grit SiCp papers. Samples were thoroughly washed and dried after each cycle of grinding. After SiCp paper grinding, the samples were cleaned with water and in the ultrasonic bath as well. Later, the samples were electropolished (STRUERS, LECTROPOL-5) using A2 Electrolyte (Composition: 90 mL water, 730 mL ethanol, 100 mL butyl cellosolve, and 78 mL perchloric acid). The samples were then cleaned with water and alcohol. The

samples were dried before placing inside the SEM chamber. The microstructures of the samples were examined using Focussed Ion Beam Scanning Electron Microscope (FIB-SEM (CARL ZEISS, AURIGA COMPACT)) machine. The samples were analyzed as per the procedure described in the literature.^[21,22] To clearly reveal the nanoparticles, initially, low-angle ion milling (10 deg) was carried out followed by slight etching using gallium ions (90 deg). SEM images were

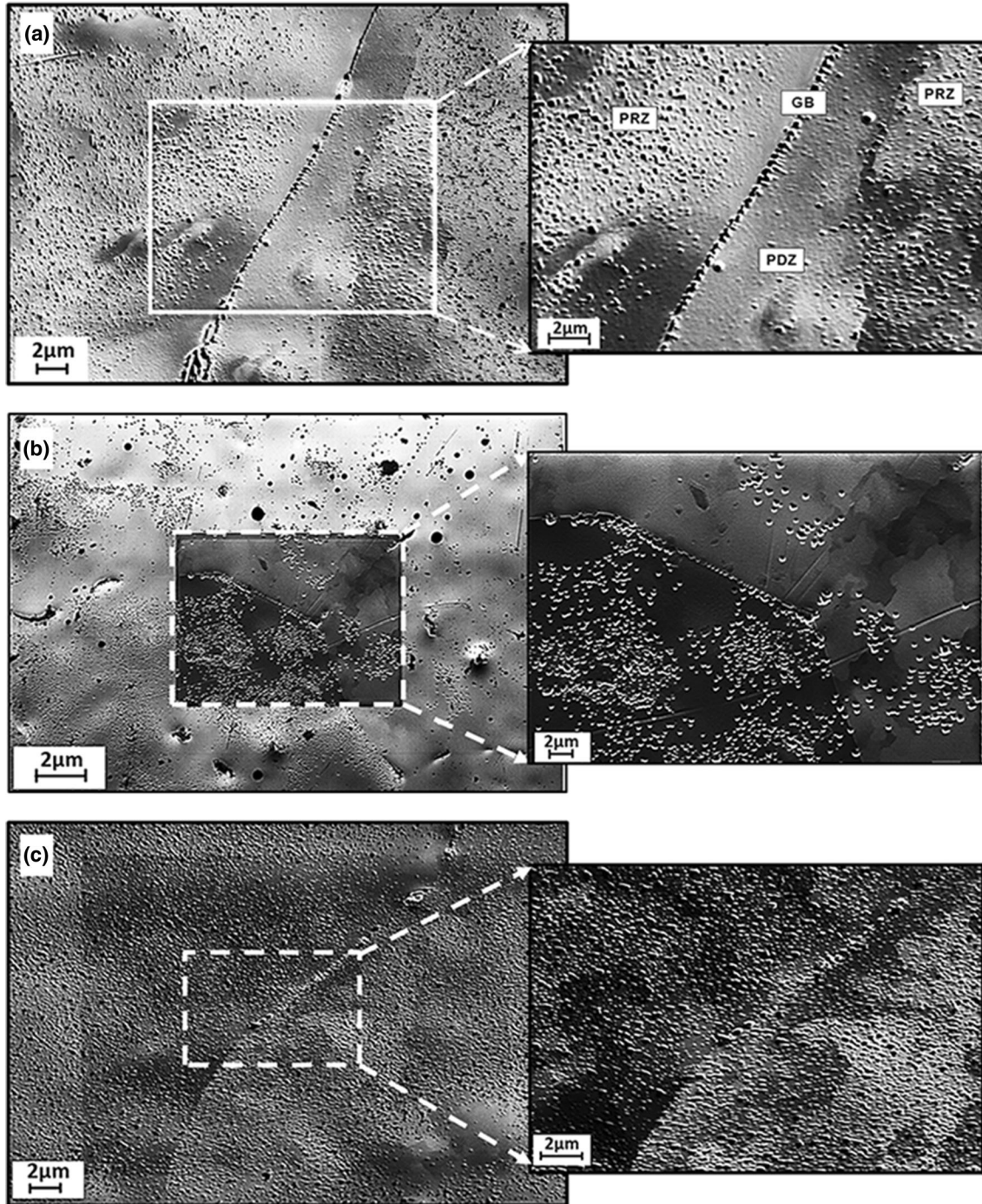


Fig. 3—FESEM micrographs of samples produced *via* ultrasonic casting in three different modes: (a) contact type (b) non-contact type (c) two-step type.

acquired at a 52 deg tilt to expose the nano-dispersoids on the surface of the aluminum matrix. EDS of the samples was carried out in order to confirm the nano-dispersoids dispersion and distribution. Samples were also examined under high-resolution TEM (JEOL, JEM-2100). The Electron Back Scattered Diffraction (EBSD) analysis of the electropolished samples was carried out with the following parameters—an area of about $(3.5 \times 4.5) \text{ mm}^2$, at a scan rate of $\sim 5 \mu/\text{s}$, and at a magnification of $\sim 50\times$. The EBSD maps were post-processed using HKL Channel 5 software for determining the grain size distribution. The tensile test of the sectioned samples was carried out on INSTRON 5900R machine and at a strain rate of 1 mm/min. The Vickers microhardness was measured in the various zones of the casting using UHLMHT hardness tester. The test was performed with a load of 100 gf and a dwell time of 15 seconds.

III. RESULTS AND DISCUSSION

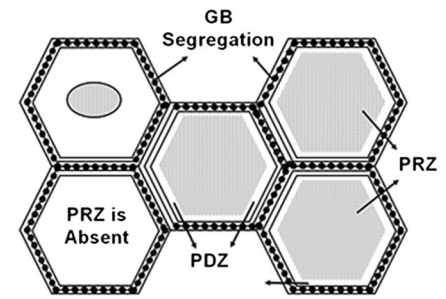
A. Effect of Two-Step Ultrasonication on Distribution of Nano-dispersoids

Figure 3(a) through (c) shows the dispersion of alumina nano-dispersoids in the aluminum matrix during contact type, non-contact type, and two-step type of ultrasonic casting. The distribution pattern of the dispersoids is very well revealed in the microstructures. The microstructures in the three cases were markedly different.

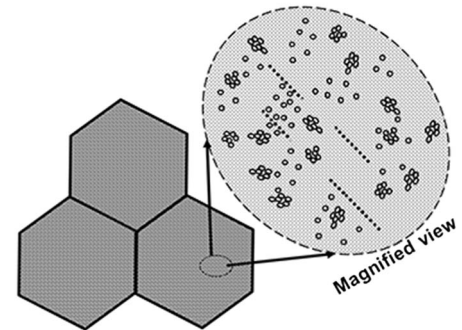
1. Microstructure in contact type

In the case of contact type ultrasonic casting, as shown in Figure 3(a), the microstructure reveals three distinguished zones namely Grain Boundary (GB); Particle-Depleted Zone (PDZ), and Particle-Reinforced Zone (PRZ). A GB is the region of segregation of Al_2O_3 dispersoids. Adjacent to the GB is the narrow PDZ where Al_2O_3 is almost absent. Next to it, inside the grain, are the PRZ, wherein the Al_2O_3 dispersoids are dispersed in the aluminum matrix. However, in some of the grains, the PRZ is either absent or is smaller sized. It is an interesting observation that the grains (or group of grains) inside which the PRZs are absent, are randomly located throughout the ingot. Moreover, these grains (or group of grains) are not only randomly distributed but are also located adjacent to those grains (or group of grains) containing PRZs. The schematic representation of the resultant microstructure is shown in Figure 4(a).

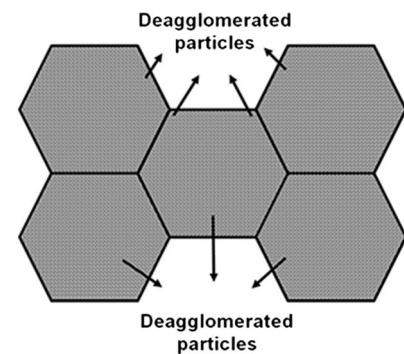
During the contact type ultrasonic casting, once the content in the crucible is melted, the top slag layer is removed and the ultrasonic probe generating high-energy waves is dipped into the melt. As the ultrasonic waves (20 kHz, 1000 W) are transmitted through the melt, cavitation and acoustic streaming take place. Alternative high-pressure (compression) and low-pressure (rarefaction) cycles are generated which results in acoustic cavitation^[3,23–26]. During this event, bubbles are nucleated in the liquid melt, which starts growing in size, pulsing in a continuous expansion–compression regime, and eventually collapses. The cavitation



(a) CONTACT TYPE



(b) NON-CONTACT TYPE



(c) TWO-STEP CONTACT-NON CONTACT TYPE

Fig. 4—Schematic representation of the microstructures observed during ultrasonic casting via three different modes: (a) contact type (b) non-contact type (c) two-step type.

generates powerful meso-scale circulatory flow that deagglomerates the clusters of nano-dispersoids. The FESEM micrographs at higher magnification reveal the deagglomeration. Once the melt treatment is completed, the liquid mixture is bottom poured into a thin stainless steel mold. No ultrasonication is provided during the solidification process and in the absence of ultrasonication, the pushing mechanism results in the GB segregation as depicted in Figure 4(a).

The pushing mechanism has been extensively studied.^[11,27–31] As the solidification begins in the liquid melt (containing nano-dispersoids), the solidification front propagates. During this event, the solid dispersoid in the liquid melt may either get engulfed by the moving solidification front or get rejected and pushed by it. Whether the dispersoid gets engulfed or pushed depends

not only upon the solidification front speed (which in turn depends upon the cooling rate) but also on the size of the dispersoid. Also, as the solidification progresses, the probability of engulfment of the dispersoid will be higher, if the solidification front speed is higher and also if the size of the dispersoid is large. But, in the case of nano-dispersoids, the size being too small, the probability of dispersoid getting pushed is higher rather than engulfment and thus engulfment would require greater front speeds.

On the other hand, as the solidification is initiated, the small dispersoids act as nucleating points and heterogeneous nucleation occurs randomly in the regions that are supercooled. However, the nucleation and grain growth are associated with the release of latent heat. The cooling rate in the liquid regions in between two newly formed grains will be lower due to the release of the latent heat, and thus, the grains formed in these regions will have comparably lower front speed resulting into

pushing. This will eventually lead to the formation of regions having grains embedded without PRZs, adjacent to, the regions having grains embedded with PRZs.

In the same line, the formation of the narrow PDZ adjacent to the GBs is possibly due to the release of the latent heat leading to the lowering of the front speed with the increase in diameter of the grain. Thus, the pushing phenomenon results in three distinguished zones depicted in Figure 4(a).

2. Microstructure in non-contact type

The microstructure observed in the case of non-contact ultrasonic casting is shown in Figure 3(b). The structure is schematically represented in Figure 4(b). It consists of a mixture of small agglomerates and deagglomerated dispersoids. Unlike in the contact type ultrasonic casting, neither the PDZs near the GBs nor the grains without PRZ are being observed. During non-contact ultrasonic casting, after the matrix material is melted, and the top

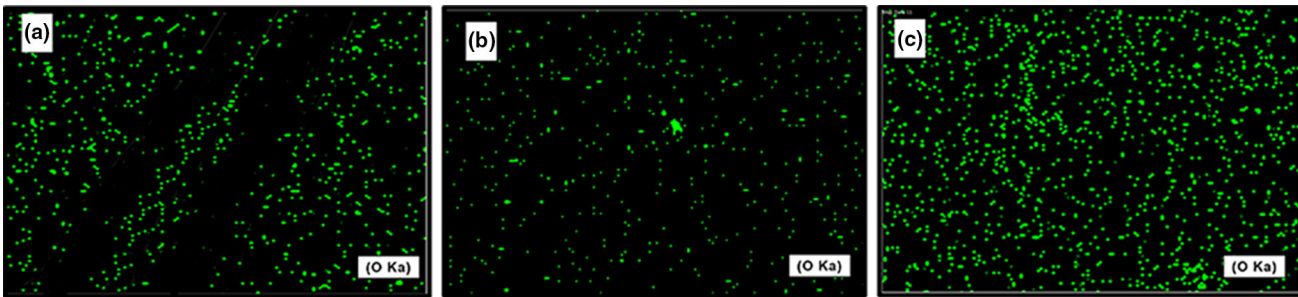


Fig. 5—EDS maps of samples produced via ultrasonic casting in three different modes: (a) contact type (b) non-contact type (c) two-step type.

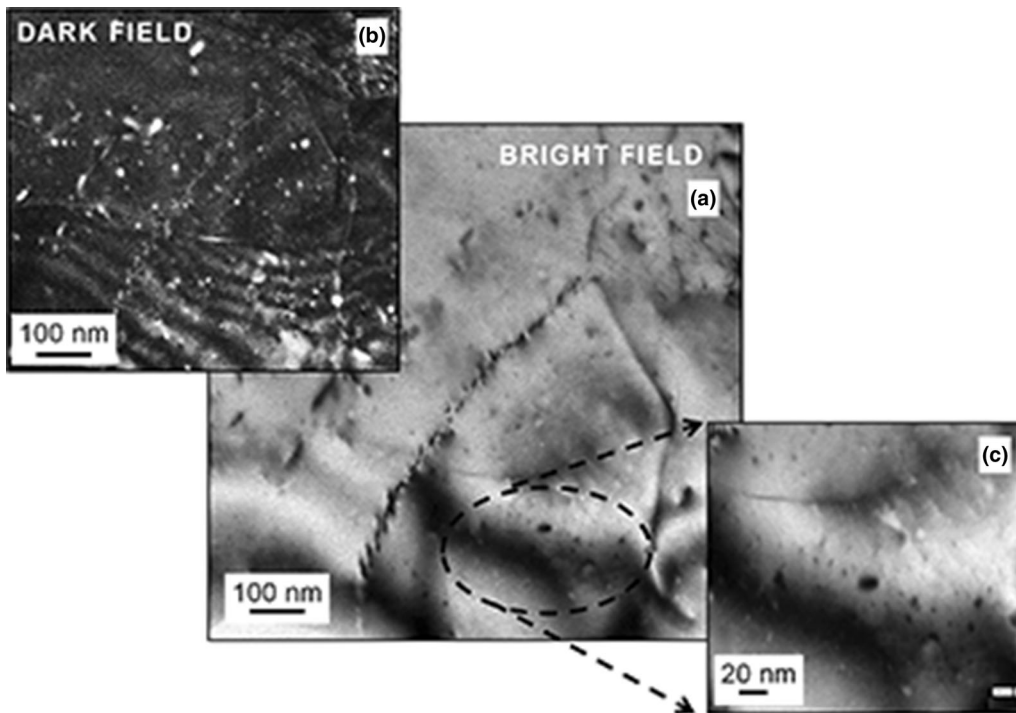


Fig. 6—TEM photograph of casting produced by two-step ultrasonic casting, (a) bright-field mode image (b) dark-field mode image (c) image at higher magnification.

oxide slag layer is removed, the nano-dispersoids are incorporated through stirring. The stirred melt is later bottom poured into the thin stainless steel mold placed in the ultrasonic chamber. The ultrasonic chamber is filled with preheated water (>80 °C) up to the top level of the mold as shown in Figure 1. The chamber consists of ultrasonic transducer that emits high-intensity waves into the water medium. During this process, both the ultrasonication and solidification take place simultaneously.

It is to be noted that ultrasonication is activated well before the melt reaches the mold and the ultrasonication is continued till the end of the solidification. These waves pervade throughout the liquid melt causing cavitation and acoustic streaming, as explained in the previous Section III-A-1. Cavitation is known to generate powerful flow circulations on the mesoscopic length scale.^[3,23-26] This will result in rapid convective heat exchange at the meso-scale, resulting in uniform cooling rate, despite the release of latent heat by the growing grains, as discussed earlier. Thus, grains without PRZ are not observed in this case.

It is quite evident that ultrasonication is more efficient, only when the contents in the mold are in the liquid state.

Thus, as the solidification starts and progresses, the intensity of the cavitation and the acoustic streaming diminish gradually. Eventually, time available for deagglomeration is less (from the time of pouring till the time significant solidification has occurred in the mold) and hence complete deagglomeration does not occur. Therefore, the microstructures at higher magnification consist of isolated nano-dispersoids as well as larger agglomerates. Mula *et al.*^[1] also reported the presence of clusters of nano-dispersoids similar to that observed in the present study and these lumps are possibly due to the difference in the cooling conditions between the present study and that carried out by Mula *et al.* These lumps are referred to as Non-Distributed Zone (NDZ) by Mula *et al.*

3. Microstructure in two-step process

The microstructure observed in the case of two-step ultrasonic casting is shown in Figure 3(c). The microstructure contains neither PDZs nor (or) least GB segregation. Complete deagglomeration and uniform distribution can be observed.

During this process, once the contents in the crucible are melted, the ultrasonic probe is dipped into the liquid

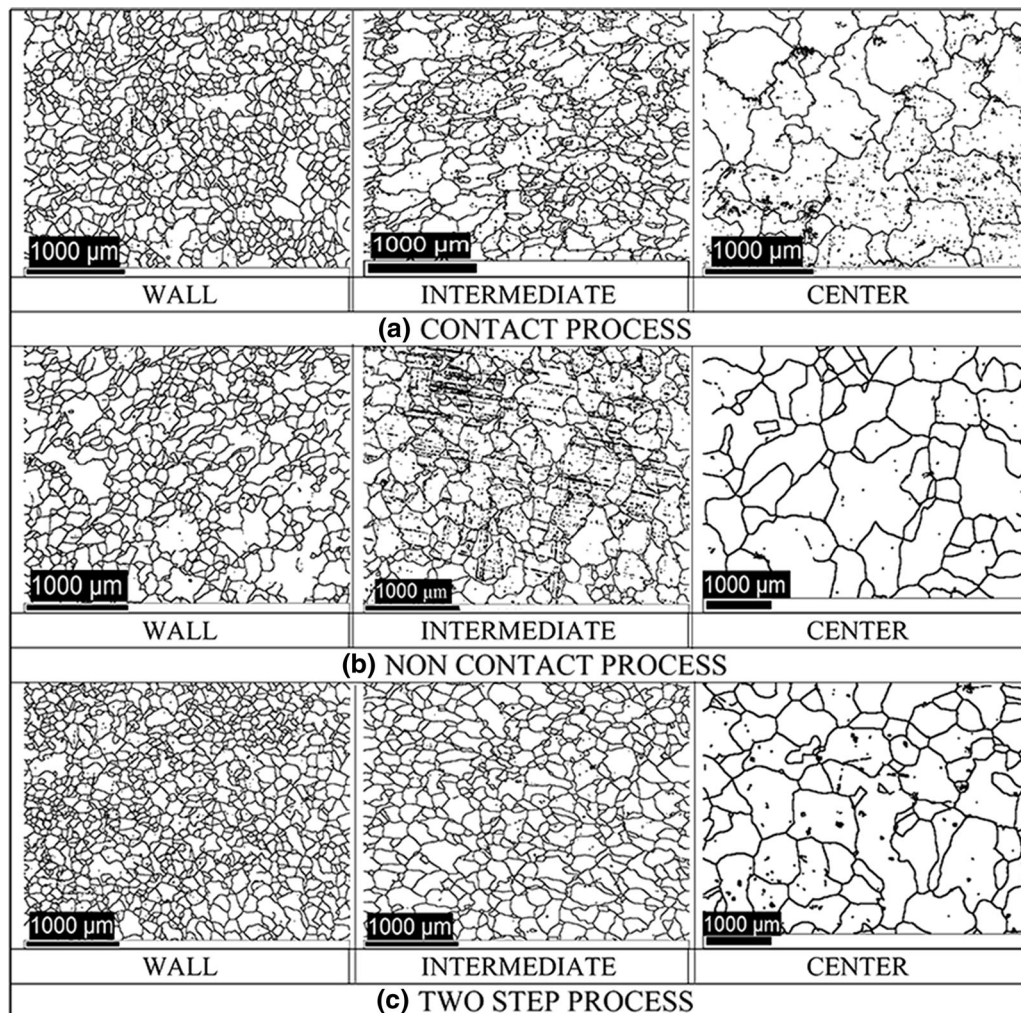


Fig. 7—EBSD maps showing the grain structures at three different zones—wall, intermediate and center, of the castings produced by three different ways: (a) contact process (b) non-contact process (c) two-step process.

melt which results into cavitation and acoustic streaming. The cavitation leads to nucleation of bubbles as explained earlier in Section III-A-1. The bubbles are able to absorb kinetic energy in the liquid melt and thus grow in size and eventually collapse. The enormous energy released during the collapse is capable enough to break the bonds between the nano-dispersoids and thus deagglomeration takes place. This results into acoustic streaming. However, acoustic streaming alone cannot help in breaking all the deagglomerates from all parts of the liquid melt, due to the obvious fact that the effective ultrasonication is limited to a small region close to the probe tip. Therefore, the external electrical stirrer is also introduced, as shown in Figure 1. The coupling of ultrasonication with stirring of the liquid melt is very much essential. The external stirring helps in moving the deagglomerated dispersoids out of the ultrasonication zone (where the ultrasonication effect is strong), while it brings the agglomerates from other parts of the liquid melt into the ultrasonication zone.

The process of deagglomeration and redistribution of dispersoids inside the liquid melt is continued for about 20 minutes. The contact type ultrasonication in combination with external stirring performs effective deagglomeration and distribution of dispersoids in the liquid melt. After 20 minutes of melt treatment, the liquid melt is bottom poured and immediately, the second step, *i.e.*, non-contact type ultrasonication is activated. The second step ultrasonication is continued till the end of

solidification. The ultrasonication during the solidification results into cavitation and acoustic streaming. During cavitation, bubbles nucleate, grow in size by undercooling the liquid melt at the dispersoid-liquid interface and eventually burst. Acoustic streaming develops in the melt, results in powerful micro-convection distributing the dispersoids in the molten melt thus promoting the heterogeneous nucleation and preventing the formation of alternate zones where there are lower cooling rates and lower front speed. It thus prevents the formation of grains without Particle-Reinforced Zones (PRZs) and also a narrow-sized Particle-Depleted Zones (PDZs) adjacent to the Grain Boundaries (GBs). This eventually results in the formation of grains without PDZ or GB segregation. The schematic representation of the resultant microstructure is shown in Figure 4(c). The EDS maps are shown in Figure 5. The oxygen distribution is clearly observed which represents the Al_2O_3 distribution.

4. TEM analysis

Further studies of the samples processed by two-step ultrasonic casting, under transmission electron microscopy, reveals the distribution very clearly. Figure 6 shows the TEM photograph.

Figure 6(a) represents the bright-field mode image which shows the absence of the GB segregation as well as the PDZ adjacent to GB. Also, the deagglomerated dispersoids are very well distributed throughout the

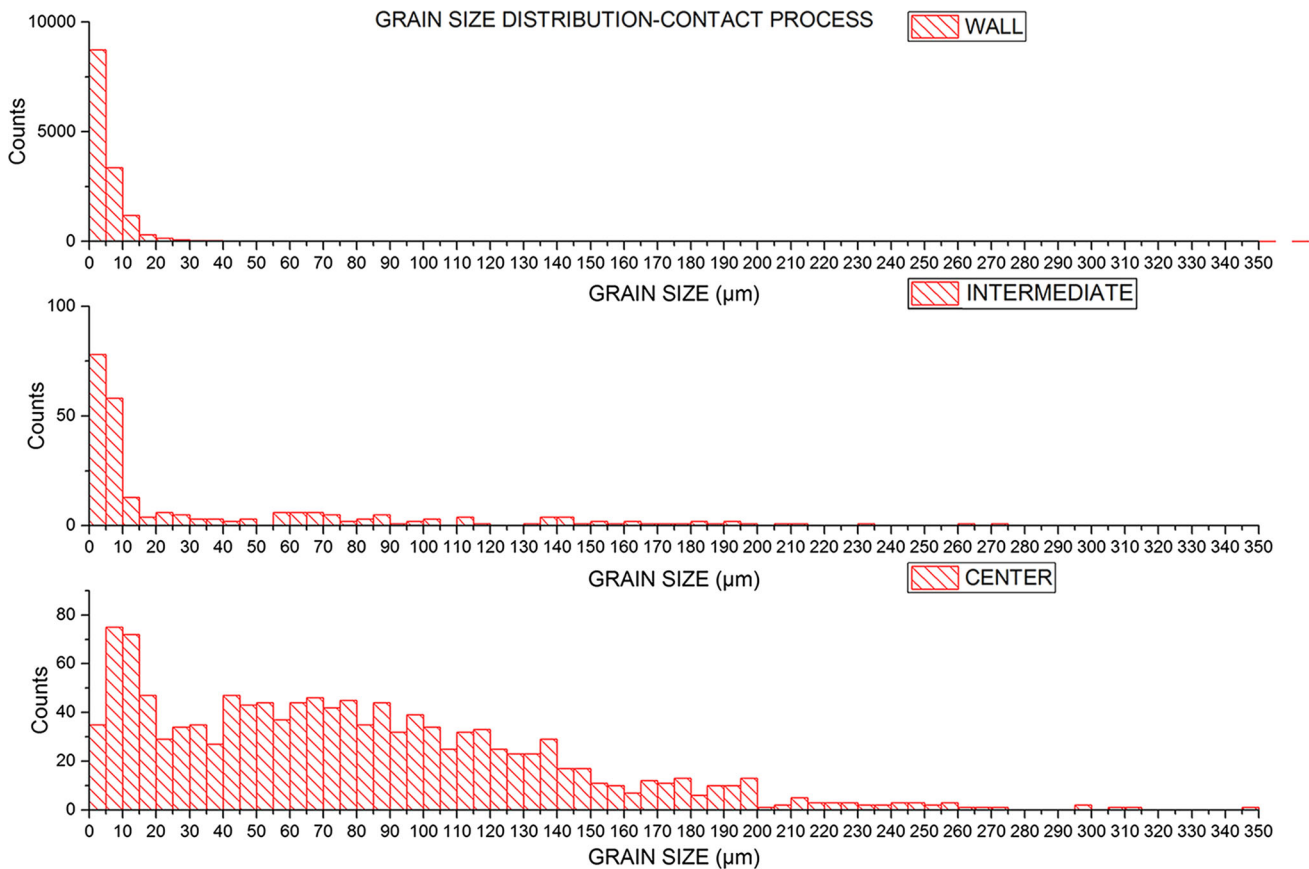


Fig. 8—Grain size distribution in the sample produced by contact process.

matrix. The dark-field mode image shown in Figure 6(b) clearly depicts the uniform distribution of nano-dispersoids. Further, at higher magnification of the inside region of the grain, as shown in Figure 6(c), it is observed that the nano-dispersoids are clearly separated and uniformly distributed. This is attributed to the avoidance of reagglomeration of the nano-dispersoids during the second step of the two-step ultrasonic casting.

B. Effect of Two-Step Ultrasonication on Grain Size Distribution

The EBSD maps of the sectioned samples (Figure 2) of the castings produced by three types of ultrasonic casting—contact, non-contact, and two-step type of ultrasonic casting are shown in Figure 7. The grain size distribution is shown in Figures 8, 9, 10. The summary of the grain size distribution is given in Table II. The variation in the grain size from the wall to the center of the casting can be clearly observed in Figure 7.

The following observations can be made from Figures 7, 8, 9, and 10 and Table II:

1. In all the three types of ultrasonic casting, the average grain size increases as one moves from wall to the center of the casting. This is due to the higher undercooling near the wall as compared to the center of the casting which is the last to solidify.

2. The average grain size achieved is the lowest in the case of two-step process. This is due to the enhanced uniform distribution of nano-dispersoids in the case of two-step ultrasonication. When the nano-dispersoid clusters are deagglomerated, each dispersoid can act as a probable site for nucleation. However, when the dispersoids segregate, each of them cannot act as an individual nucleating site.
3. In the case of two-step process, in each zone, a maximum number of grains (80, 60, and 55 pct) are of a nearly same size as compared to that of contact and non-contact process. Thus, it can be said that most of the grains formed are because of the increased number of nucleating sites. These nucleating sites indicate proper deagglomeration and also the uniform distribution.
4. In the case of two-step process, ~80 pct of the grains near the wall side are of $\leq 5 \mu\text{m}$ in size. This implies that a maximum number of grains are uniformly distributed, and only 20 pct are of other sizes.
5. In the case of contact process, only 45 pct are in the range of $\leq 5 \mu\text{m}$, the remaining 55 pct of the grains are of different sizes. This clearly indicates, the grains with uniform grain sizes are not formed. The same is in the case of non-contact type process. This also indicates that the dispersoids at few regions, *i.e.*, PRZs are absent (Figure 4(a)).

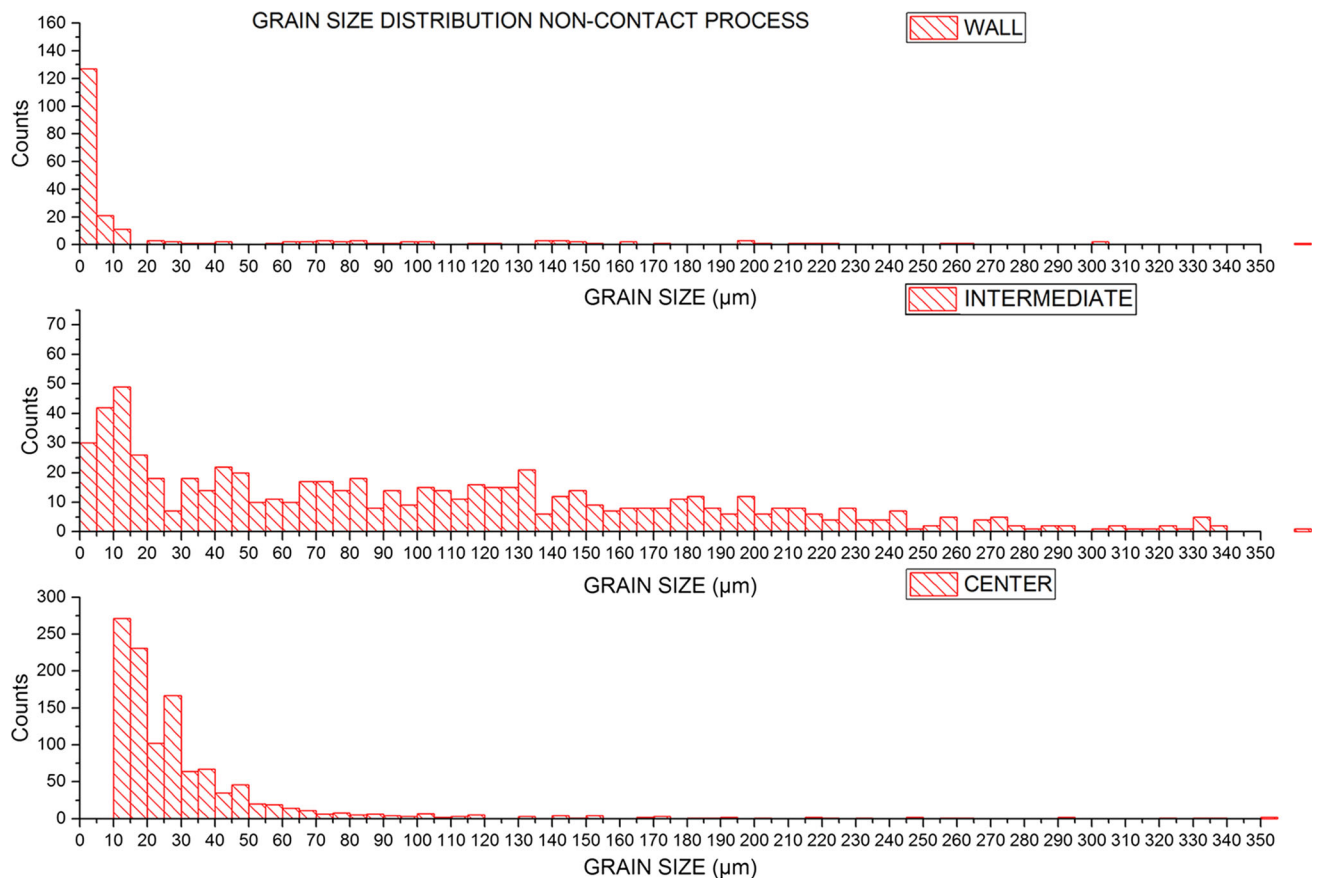


Fig. 9—Grain size distribution in the sample produced by non-contact process.

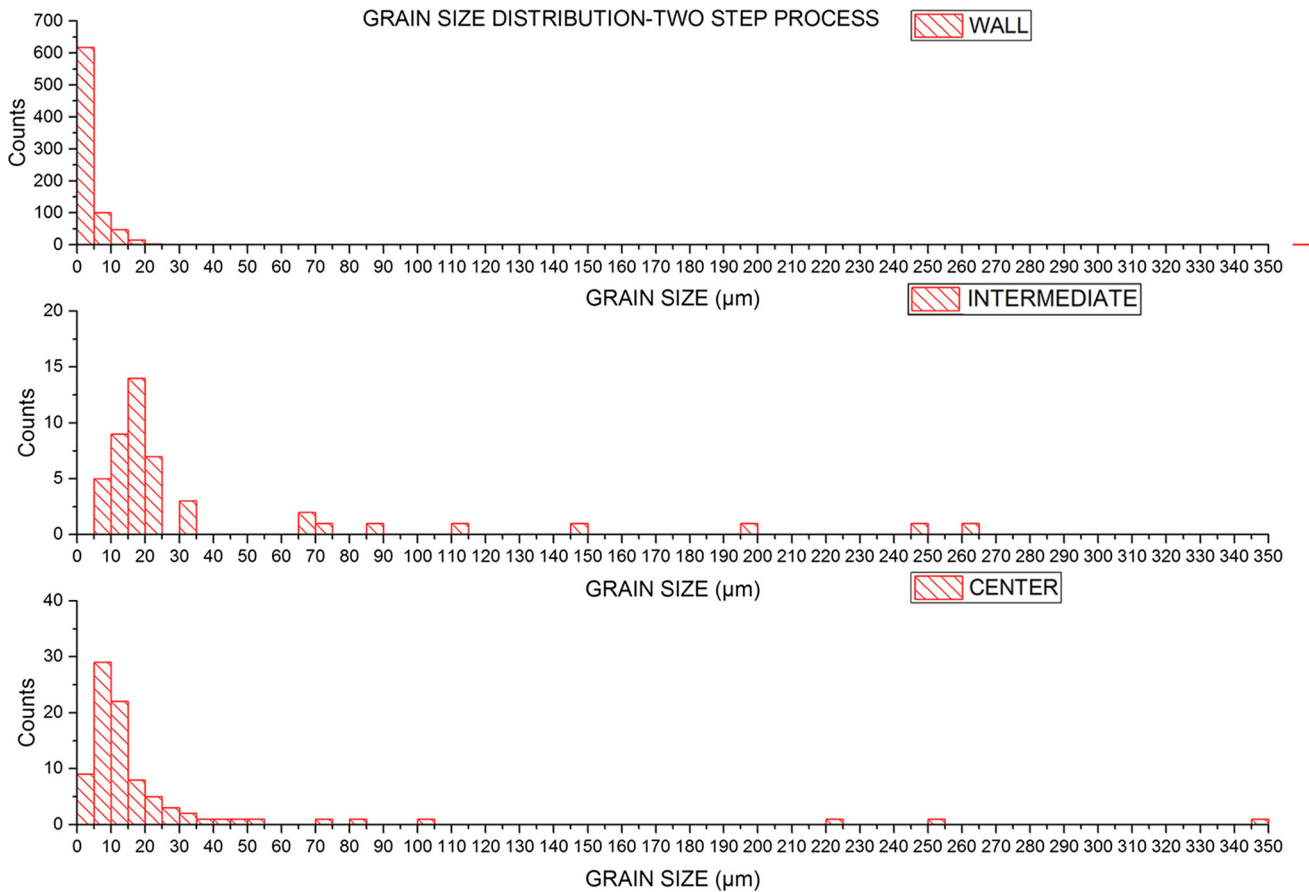


Fig. 10—Grain size distribution in the sample produced by two-step process.

Table II. Summary of the Grain Size Distribution

Zone	Contact			Non-Contact			Two-Step		
	Distribution		Average Grain Size (μm)	Distribution		Average Grain Size (μm)	Distribution		Average Grain Size (μm)
	Grain Size (μm)	Percentage of Grains		grain size (μm)	Percentage of Grains		Grain Size (μm)	Percentage of Grains	
Wall	≤ 5	60	170	≤ 5	45	156	≤ 5	80	140
Intermediate	10-30	20	214	10-30	20	199	10-30	60	163
Center	30-50	10	254	30-50	55	209	30-50	55	204

C. Effect of Two-Step Ultrasonication on Mechanical Properties

The variation of average microhardness at different zones of the cast ingots is shown in Figure 11. An average of about 25 data points has been reported for each zone. The average microhardness (averaged over all zones) in the case of two-step process is higher than those achieved in contact and non-contact process. The error bar in Figure 11 clearly indicates the variation. As we move from one to another zone (Figure 2), the variation of microhardness is the maximum in the case of the non-contact process and is the minimum in the case of the two-step process. This indicates the possibility of enhanced distribution of nano-dispersoids in the case of two-step process, leading to fine grains as a result

of increased nucleating sites and thus indicates the nearly uniform hardness throughout the casting.

The stress-strain plots obtained from the tensile tests of the bulk nanocomposites produced via three types of ultrasonic casting processes are shown in Figure 12. The samples for the tensile testing are cut vertically from the center of the casting. The tensile strength is calculated using 0.2 pct strain offset method.^[32] The tensile strength achieved in the two-step process is higher than those produced by the other two types of ultrasonic casting methods. The increment is ~9 pct as compared to the non-contact process and about ~14 pct as compared to contact process.

The variation of yield strength of the nanocomposites produced by three different processes is shown in

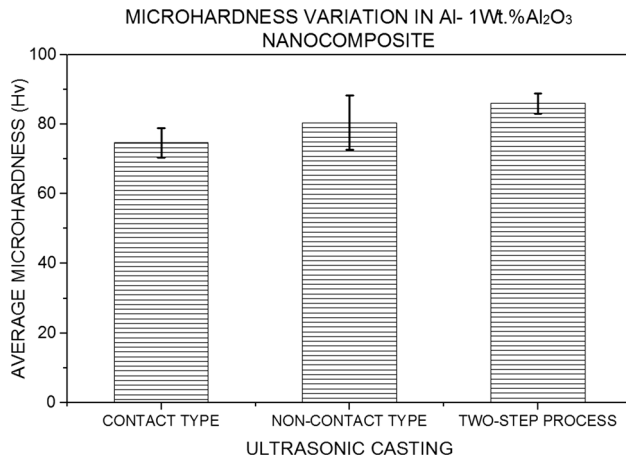


Fig. 11—Average microhardness of samples produced by contact type, non-contact type, and two-step type of ultrasonic casting.

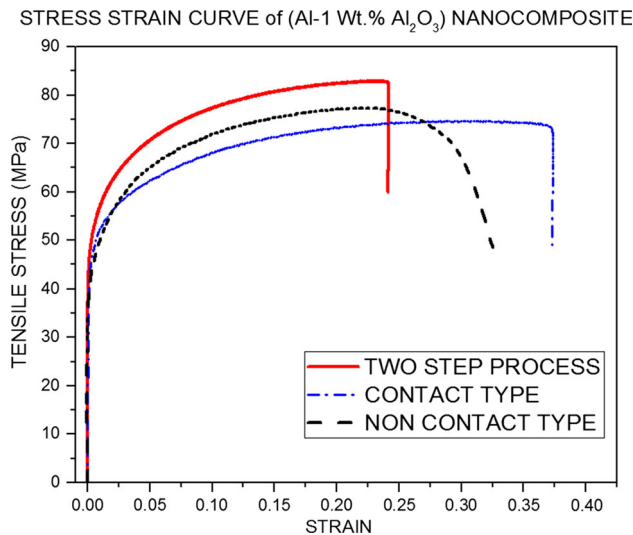


Fig. 12—Stress–strain curves for Al-1 wt pct Al₂O₃ nanocomposites produced by contact type, non-contact type, and two-step type of ultrasonic casting.

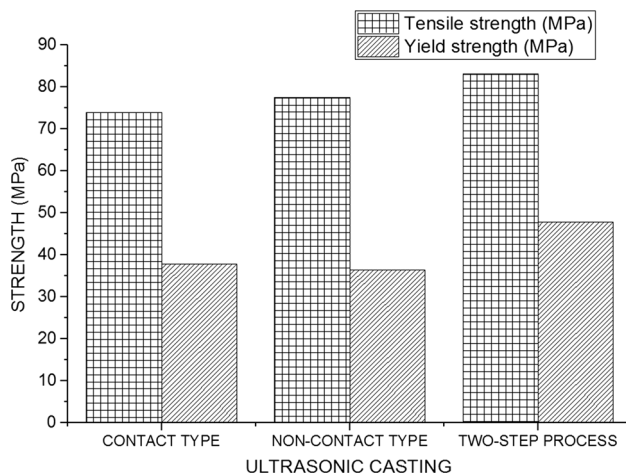


Fig. 13—Tensile test results of Al-1 wt pct Al₂O₃ nanocomposites produced by contact type, non-contact type, and two-step type of ultrasonic casting.

Figure 13. The yield strength achieved in the case of two-step process is ~50 MPa and in the case of contact and non-contact process, it is ~39 MPa and ~38 MPa, respectively. The increment in the yield strength of the two-step process is ~32 pct as compared to the contact and non-contact process. It is to be noted that the yield strength of the Al-2 wt pct Al₂O₃ nanocomposite produced by non-contact process adopted by Mula *et al.*^[1] was 47 MPa. The Al-1 wt pct Al₂O₃ nanocomposite produced by the non-contact process adopted in the current study exhibited a yield strength of ~39MPa.

The yield strength of the nanocomposite produced by two-step process will be influenced by the Hall–Petch strengthening as well as the nano-dispersion strengthening. The Hall–Petch relationship^[32] is as follows:

$$\sigma_y = \sigma_0 + \frac{k_y}{\sqrt{d}},$$

where ‘ σ_y ’ is the yield stress, ‘ σ_0 ’ is a material constant, ‘ k_y ’ is the strengthening coefficient, and ‘ d ’ is the average grain diameter. Table II shows the average grain sizes of the castings produced by contact, non-contact, and the two-step processes. It is evident from the table that the grain sizes of the nanocomposites are comparable. A ~38 pct higher yield strength is observed in the nanocomposite produced by two-step process, which is possibly due to the improved nano-dispersion strengthening.

IV. CONCLUSIONS

The following are the conclusions drawn out of the present study:

1. Al-Al₂O₃ bulk MMNCs were successfully cast through a two-step ultrasonic casting technique that combines contact type ultrasonication, external stirring, bottom pouring, and non-contact type ultrasonication during solidification. The contact type ultrasonication combined with stirring results in complete deagglomeration of nano-dispersoid clusters as a result of cavitation and redistribution of the clusters/deagglomerated dispersoids within the liquid melt. However, during the subsequent casting during contact type, zones of lower cooling rate (where the nano-dispersoids were pushed to the grain boundary regions) were formed due to the release of latent heat from adjacent solidification regions. In the case of the two-step process, the particle-depleted zones were not observed resulting in unprecedented uniformity. This is possibly due to cavitation and powerful micro-convection during the solidification that circumvents non-uniformity in the cooling rate at the meso-scale.
2. Tensile testing of the nanocomposite revealed that the yield strength of the nanocomposite produced by the two-step process was ~38 pct higher than that produced by non-contact and contact methods. Careful microstructural analysis using EBSD suggests that the higher yield strength is due to the

more uniform distribution of the nano-dispersoids in the nanocomposite produced by the two-step process.

ACKNOWLEDGMENTS

This work was supported by the National Institute of Ocean Technology, Chennai, Ministry of Earth Sciences, New Delhi, INDIA, and the work was carried out at Indian Institute of Technology Kharagpur, INDIA.

REFERENCES

1. S. Mula, P. Padhi, S.C. Panigrahi, S.K. Pabi, and S. Ghosh: *Mater. Res. Bull.*, 2009, vol. 44, pp. 1154–60.
2. S. Mula, S.K. Pabi, C.C. Koch, P. Padhi, and S. Ghosh: *Mater. Sci. Eng. A*, 2012, vol. 558, pp. 485–91.
3. P. Padhi, K.N. Kumar, S. Ghosh, H.M. Vishwanatha, S.C. Panigrahi, and S. Ghosh: *Mater. Manuf. Process.*, 2015, vol. 0, pp. 1–8. 10.1080/10426914.2015.1004707.
4. R.S. Rana, R. Purohit, and S. Das: *Int. J. Sci. Eng. Res.*, 2012, vol. 3, pp. 1–16.
5. L.Y. Chen, J.Y. Peng, J.Q. Xu, H. Choi, and X.C. Li: *Scr. Mater.*, 2013, vol. 69, pp. 634–37.
6. L.Y. Chen, D. Weiss, J. Morrow, J.Q. Xu, and X.C. Li: *Manuf. Lett.*, 2013, vol. 1, pp. 62–65.
7. J. Hashim, L. Looney, and M.S.J. Hashmi: *J. Mater. Process. Technol.*, 1999, vols. 92–3, pp. 1–7.
8. S.A. Sajjadi, H.R. Ezatpour, and H. Beygi: *Mater. Sci. Eng. A*, 2011, vol. 528, pp. 8765–71.
9. C. Suryanarayana, E. Ivanov, and V. Boldyrev: *Mater. Sci. Eng., A*, 2001, vols. 304–306, pp. 151–58.
10. H. Gleiter: *Acta Mater.*, 2000, vol. 48, pp. 1–29.
11. J.Q. Xu, L.Y. Chen, H. Choi, and X.C. Li: *J. Phys.: Condens. Matter*, 2012, vol. 24, pp. 255304–255314.
12. G.I. Eskin: *Adv. Perform. Mater.*, 1997, vol. 1, pp. 223–32.
13. M. De Cicco, H. Konishi, G. Cao, H.S. Choi, L.S. Turng, J.H. Perepezko, S. Kou, R. Lakes, and X. Li: *Metall. Mater. Trans. A*, 2009, vol. 40A, pp. 3038–45.
14. S.A. Vorozhtsov, D.G. Eskin, J. Tamayo, A.B. Vorozhtsov, V.V. Promakhov, A.A. Averin, and A.P. Khrustalyov: *Metall. Mater. Trans. A*, 2015, vol. 46A, pp. 2870–75.
15. G. Cao, J. Kobliska, H. Konishi, and X. Li: *Metall. Mater. Trans. A*, 2008, vol. 39A, pp. 880–86.
16. H. Choi, M. Jones, H. Konishi, and X. Li: *Metall. Mater. Trans. A*, 2012, vol. 43A, pp. 738–46.
17. Y. Yang, J. Lan, and X. Li: *Mater. Sci. Eng., A*, 2004, vol. 380, pp. 378–83.
18. N. Srivastava and G.P. Chaudhari: *Mater. Sci. Eng., A*, 2016, vol. 651, pp. 241–47.
19. S. Kandemir, D.P. Weston, and H.V. Atkinson: *Key Eng. Mater.*, 2012, vols. 504–506, pp. 339–44.
20. H. Ribes, R. Da Silva, M. Suéry, and T. Bretheau: *Mater. Sci. Technol.*, 1990, vol. 6, pp. 621–28.
21. L.-Y. Chen, J.-Q. Xu, and X.-C. Li: *Mater. Res. Lett.*, 2015, vol. 3, pp. 43–49.
22. L.-Y. Chen, J.-Q. Xu, H. Choi, M. Pozuelo, X. Ma, S. Bhowmick, J.-M. Yang, S. Mathaudhu, and X.-C. Li: *Nature*, 2015, vol. 528, pp. 539–43.
23. G.I. Eskin: *Ultrason. Sonochem.*, 2001, vol. 8, pp. 319–25.
24. G.I. Eskin and D.G. Eskin: *Ultrason. Sonochem.*, 2003, vol. 10, pp. 297–301.
25. T. Hielscher: *ENS' 05 Paris*, France, Paris, 2005, pp. 1–6.
26. A. Ramirez, M. Qian, B. Davis, T. Wilks, and D.H. StJohn: *Scr. Mater.*, 2008, vol. 59, pp. 19–22.
27. Y.M. Youssef, R.J. Dashwood, and P.D. Lee: *Compos. Part A*, 2005, vol. 36A, pp. 747–63.
28. S. Sen, B.K. Dhindaw, D.M. Stefanescu, A. Catalina, and P.A. Curreli: *J. Cryst. Growth*, 1997, vol. 173, pp. 574–84.
29. F.R. Juretzko, B.K. Dhindaw, D.M. Stefanescu, S. Sen, and P.A. Curreli: *Metall. Mater. Trans. A*, 1998, vol. 29A, pp. 1691–96.
30. D.M. Stefanescu, F.R. Juretzko, B.K. Dhindaw, A. Catalina, and S. Sen: *Metall. Mater. Trans. A*, 1998, vol. 29A, pp. 1697–1706.
31. J.B. Ferguson, G. Kaptay, B.F. Schultz, P.K. Rohatgi, K. Cho, and C.S. Kim: *Metall. Mater. Trans. A*, 2014, vol. 45A, pp. 4635–45.
32. E. George: *Dieter: Mechanical Metallurgy*, 2nd ed., McGraw-Hill book Co., New York, 1988.